BIOCHEMISTRY
including biophysical chemistry & molecular biology

Article

pubs.acs.org/biochemistry

A Physicochemical and Mutational Analysis of Intersubunit Interactions of *Escherichia coli* Ferritin A

Hideaki Ohtomo,[†,§] Mio Ohtomo,[†] Daisuke Sato,[†] Atsushi Kurobe,[†] Ayumi Sunato,[†] Yoshitaka Matsumura,[‡,∥] Hiroshi Kihara,[‡] Kazuo Fujiwara,[†] and Masamichi Ikeguchi*[,†]

[†]Department of Bioinformatics, Soka University, 1-236 Tangi-cho, Hachioji, Tokyo 192-8577, Japan

[‡]Department of Physics, Kansai Medical University, 18-89 Uyama-Higashi, Hirakata 573-1136, Japan

Supporting Information

ABSTRACT: Ferritin A from *Escherichia coli* (EcFtnA) is 24-meric protein, which forms spherical cagelike structures called nanocages. The nanocage structure is stabilized by the interface around 4-, 3-, and 2-fold symmetric axes. The subunit structure of EcFtnA comprises a four-helix bundle (helices A−D) and an additional helix E, which forms a 4-fold axis. In this study, we examined the contribution of the interface around three symmetric axes. pH-induced dissociation experiments monitored by analytical ultracentrifugation and small-angle X-ray scattering showed that the dimer related by 2-fold symmetry is the most stable unit. Mutations located near the 3-fold axis revealed that the contribution of each interaction was small. A mutant lacking helix E at the 4-fold axis formed a nanocage, suggesting that helix E is not essential for nanocage formation. Further truncation of the C-terminus of helix D abrogated the formation of the nanocage, suggesting that a few residues located at the C-terminus of helix D are critical for this process. These properties are similar to those known for mammalian ferritins and seem to be common principles for nanocage formation. The difference between EcFtnA and mammalian ferritins was that helix E-truncated EcFtnA maintained an iron-incorporating ability, whereas mammalian mutants lost it.

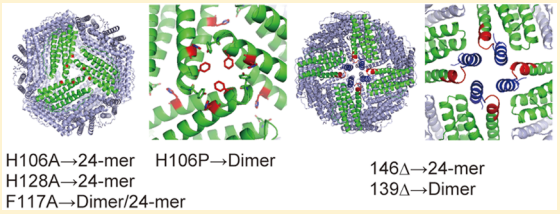

Ferritins are oligomeric proteins that can form a nanocage structure whose main functions are storing and detoxifying intracellular iron.[1−4] Because of their characteristic structure and ability to bind various metals, ferritins have been studied in the field of macromolecular assembly and nanomaterial design.[5−8] Ferritins can be categorized as heme-binding bacterioferritins (Bfrs), non-heme-binding ferritins, and 12-meric ferritins. Both Bfrs and non-heme-binding ferritins form a 24-meric nanocage structure with octahedral 432 symmetry. By contrast, 12-meric ferritins form 12-meric nanocages with tetrahedral 332 symmetry. The 12-meric ferritin contains DNA-binding protein from starved cells (Dps) and Dps-like ferritin. Bfr and 12-meric ferritin are found in prokaryotes, whereas non-heme-binding ferritins are found extensively in prokaryotes and eukaryotes.

Mammalian cytosolic ferritins comprise two subunit types, named the H and L chains, with ∼50% amino acid sequence identity, which assemble into 24-mers in different proportions. Ferritins from different species can form hybrid 24-mers by mixing and reassembling the dissociated subunits.[9] These properties of ferritins indicate that the interactions between the subunits are very flexible. To understand the mechanisms of ferritin assembly and to design an artificial nanocage structure, further knowledge of these flexible interactions is needed. The important residues for assembly have been identified by mutational analyses for *Mycobacterium tuberculosis* Bfr,[10] *Escherichia coli* Bfr,[11] and Dps.[12] Extensive mutational analyses have also been used to study non-heme-binding human ferritins.[13−15] Despite these efforts, the general mechanisms by which flexible and stable cage structures are formed are not fully understood.

In this study, we investigated the intersubunit interactions of *E. coli* ferritin A (EcFtnA), a type of non-heme-binding ferritin (Figure 1). In contrast to mammalian ferritins, EcFtnA comprises 24 identical subunits, whose three-dimensional structure is similar to that of chain H of human ferritin (HuHF).[16] However, interactions between subunits related by 2-, 3-, and 4-fold axes differ significantly between EcFtnA and HuHF.[16] For example, the interaction around the 3-fold axis is hydrophobic in *E. coli* ferritin, whereas it is mainly electrostatic in human ferritin. Therefore, it is interesting to compare the intersubunit interactions between EcFtnA and HuHF. First, we examined the pH dependence of higher-order structures of EcFtnA because it has been shown that the dimeric state in horse[17,18] and human[19] ferritins is stable under acidic conditions. Next, we constructed several ferritin mutants, in which residues at the interface near the 3-fold axis were substituted. Two C-terminally truncated mutants were also constructed to examine the role of helix E in the 4-fold axis. The abilities for 24-mer formation and iron storage were investigated for these mutants.

Received: June 27, 2015
Revised: September 22, 2015
Published: September 24, 2015

DOI: 10.1021/acs.biochem.5b00723
Biochemistry 2015, 54, 6243−6251

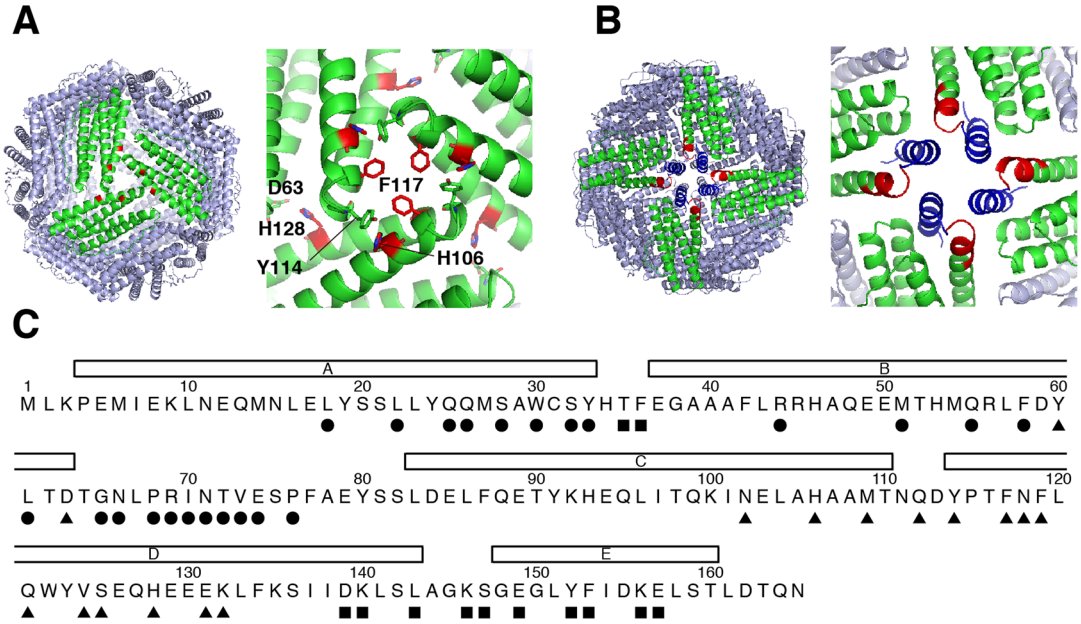

Figure 1. Interface near the (A) 3-fold axis and (B) 4-fold axis (PDB entry 1EUM[16]). (A) His106, Phe117, and His128 are colored red. (B) Residues 139−145 and 146−165 are colored red and blue, respectively. (C) Amino acid sequence of EcFtnA. Secondary structural elements are indicated above the sequence; the rectangles labeled A−E represent α-helices. The symbols below the sequences indicate the residues of the interface near the 2-fold axis (●), 3-fold axis (▲), and 4-fold axis (■).

MATERIALS AND METHODS

Construction of a Gene Encoding Ferritin and Its Mutants. The EcFtnA gene was initially amplified from genomic DNA of *E. coli* strain B by polymerase chain reaction (PCR) with a pair of synthetic oligonucleotides containing an *Nde*I site just before the N-terminal coding sequence and a *Bam*HI site just after the termination codon. The amplified gene was inserted into an *Eco*RV site of pBluescript II (Agilent Technologies). Because the EcFtnA gene has an internal *Nde*I site in the middle of the sequence, this was eliminated by changing codon CAT to CAC. The gene was digested with *Nde*I and *Bam*HI and inserted into expression vector pET 3c. The mutants (H106A, H106P, F117A, and H128A) were constructed by site-directed mutagenesis using a QuikChange kit (Agilent Technologies). The truncated mutants (139Δ and 146Δ) were constructed using PCR with oligonucleotide primers containing a termination codon at the desired position. DNA sequences were confirmed using an ABI PRISM 3100-Avant sequencer. After sequence confirmation, *E. coli* BL21-(DE3) was transformed with the expression plasmids.

Expression and Purification of Ferritin and Its Mutants. *E. coli* harboring the expression plasmid was grown in Luria-Bertani medium, and protein expression was induced by addition of 0.1 mM isopropyl β-D-thiogalactopyranoside. EcFtnA and its mutants were found in the soluble fractions of the cell lysate. For wild-type EcFtnA (WT), H106A, H128A, and 146Δ, the crude soluble fractions were heated to 70−75 °C for 5 min and then cooled rapidly to 4 °C. The precipitate formed was removed by centrifugation. This process was omitted during preparation of H106P, F117A, and 139Δ. The pH of the supernatant was adjusted to 5.5, and polyethylenimine [0−0.1% (v/v)] was added to precipitate nucleic acids. The proteins in the supernatants were precipitated by ammonium sulfate (30−50% saturation), collected by centrifugation, and dissolved in 50 mM Tris-HCl (pH 8.0). The proteins were purified by gel filtration chromatography using a Sephacryl S300 column at pH 8.0. Fractions containing ferritins were purified further using Q-Sepharose chromatography in 50 mM Tris-HCl (pH 8.0) with a linear gradient from 0.1 to 0.6 M NaCl. Fractions containing pure proteins were dialyzed against 1 mM sodium phosphate (pH 7.0). The purity of proteins was confirmed by sodium dodecyl sulfate−polyacrylamide gel electrophoresis (SDS−PAGE) (14% acrylamide) and native PAGE (7% acrylamide).

CD Spectroscopy. CD spectra were recorded using a Jasco J-720 spectropolarimeter or an Applied Photophysics Chirascan CD spectrometer. Near- and far-UV CD spectra were obtained with cuvettes with path lengths of 10 and 1 mm, respectively. The protein concentration, as determined by ultraviolet spectroscopy, was 0.2−0.6 mg/mL. An extinction coefficient (ε_{280}) of 24000 M^{-1} cm^{-1} was used for WT, H106A, H106P, F117A, and H128A, and an ε_{280} of 22800 M^{-1} cm^{-1} was used for the truncated mutants (139Δ and 146Δ). These values were determined using the method of Gill and von Hippel.[20]

Sedimentation Velocity. Sedimentation velocity experiments were performed using a Beckman XL-I analytical ultracentrifuge and an An-50 Ti rotor at 20 °C and 30000 or 40000 rpm. The solution conditions were 10 mM sodium phosphate containing 200 mM NaCl (pH 7.0 or 3.0) and 50 mM sodium phosphate (pH 7.0 or 3.0). Sedimentation of the proteins was monitored at 280 nm at 1 min (24-meric form) or 2 min (dimeric form) intervals using a radial step size of 0.003 cm. The protein concentration was 0.2−1.2 mg/mL. Data were analyzed using SEDFIT 12.1.[21]

Analytical Gel Filtration Chromatography. Samples in 10 mM sodium phosphate containing 200 mM NaCl (pH 7.0) were loaded onto a column of Superose 6 (GE Healthcare) and eluted at a flow rate of 0.4 mL/min. The elution was monitored by UV absorbance at 280 nm.

Small-Angle X-ray Scattering. Small-angle X-ray scattering (SAXS) measurements were performed at BL15A or BL6A of the Photon Factory at the High Energy Accelerator Research

DOI: 10.1021/acs.biochem.5b00723
Biochemistry 2015, 54, 6243−6251

Organization (Tsukuba, Japan) and at BL45XU of SPring-8 (Hyogo, Japan). The X-ray wavelength was 1.5 Å (Photon Factory) or 1.0 Å (SPring-8). The camera length was 1.5 or 2 m. Scattering profiles were collected by a two-dimensional charge-coupled device (CCD)-based X-ray detector at the Photon Factory and imaging plate area detector R-AXIS II/IV++ or a Pilatus 300K at BL45XU. The scattering vector $Q = (4\pi/\lambda) \sin \theta$, where λ is the wavelength and 2θ is the scattering angle, was calibrated with the meridional diffraction of dried collagen or with a powder diffraction of silver behenate. To minimize the effect of X-ray radiation damage on the scattering data, a flow cell was used at BL15A, as described previously,[22] and at BL45XU, the sample cell was moved vertically or horizontally during exposure. The typical exposure time was 1−1.5 s; 36−50 two-dimensional images were acquired and stored separately and were averaged after the absence of any marked intensity change because of aggregation had been confirmed. The temperature was controlled at 25 °C by circulating water from a thermostat bath. To obtain one-dimensional scattering data, CCD images were processed as described previously.[23] Two-dimensional images of R-AXIS were circularly integrated using FIT2D.[24] The radius of gyration, R_g, was obtained using the Guinier approximation:

$$\ln I(Q) = \ln I(0) - \frac{R_g^2 Q^2}{3} \quad (1)$$

where $I(Q)$ is the scattering intensity at a given Q value and $I(0)$ is the forward scattering intensity. The R_g value was calculated from the slope of the Guinier plot in the ranges of $Q < 0.026$ for the 24-mer and $Q < 0.056$ for the dimer.

Iron Incorporation Assay with Prussian Blue Staining. Approximately 2 mg/mL of each protein in 50 mM PIPES (pH 6.5) was incubated with 1 mM iron(II) chloride. The reaction mixtures were incubated for 3 h at room temperature to allow Fe(II) oxidation and subsequent incorporation as Fe(III) into the protein shell. The reaction mixtures were separated by native PAGE (7% acrylamide) and stained with Coomassie brilliant blue (protein staining) and Prussian blue (iron staining). In the latter assay, 1% potassium hexacyanoferrate(II) in 75 mM HCl specifically forms a blue coordination complex with Fe(III) (Prussian blue staining). The gel was incubated with Prussian blue stain for 20−30 min, after which excess stain was removed by washing with water.

RESULTS

pH-Dependent Structural Change in EcFtnA. Horse and human ferritins dissociate into dimers at acidic pH.[17−19] It has been predicted from the crystal structure of the 24-mer that the dyad-related dimer is stable.[25] To determine whether this is the case for EcFtnA, we performed the sedimentation velocity experiment in the pH range of 2−8. The sedimentation coefficient (s) of EcFtnA was constant between pH 4 and 8 and decreased sharply between pH 4 and 3 (Figure 2A). The values of the sedimentation coefficients were 15.24 and 2.94 S at pH 7 and 3, respectively (Table 1). The molecular weights were estimated to be 466000 and 39000, respectively, indicating that EcFtnA formed a 24-meric nanocage at pH 7 and a dimer at pH 3. This behavior is similar to that observed for mammalian ferritins.[17−19] In the 24-meric crystal structure,[16] each subunit made contact with five neighbors (Figure S1). Assuming that a pair of subunits in contact within the 24-mer keeps their contact in the acid-dissociated state, five dimeric structures are possible (AC, AD, AF, AO, and AX; the letters identifying the subunits are based on the OLIGAMI database[26]). Of these five dimers, AC and AX have the same shape, and AD and AO do also. Of these possibilities, a dyad-related dimer (AF) was predicted to be stable because it has the widest contact area.[25] To confirm this prediction, we used SAXS of EcFtnA under neutral and acidic pH conditions. Figure 2B shows the Guinier plot of EcFtnA at pH 7 and 2.5. The radii of gyration were estimated from the slopes of this figure in a low-Q range (54.1 Å at pH 7 and 23.2 Å at pH 2.5). The former value is consistent with the value of 53.8 Å, which was calculated from the known crystal structure of the 24-mer[16] using CRYSOL.[27] The radius of gyration of the dyad-related dimer was calculated to be 22.7

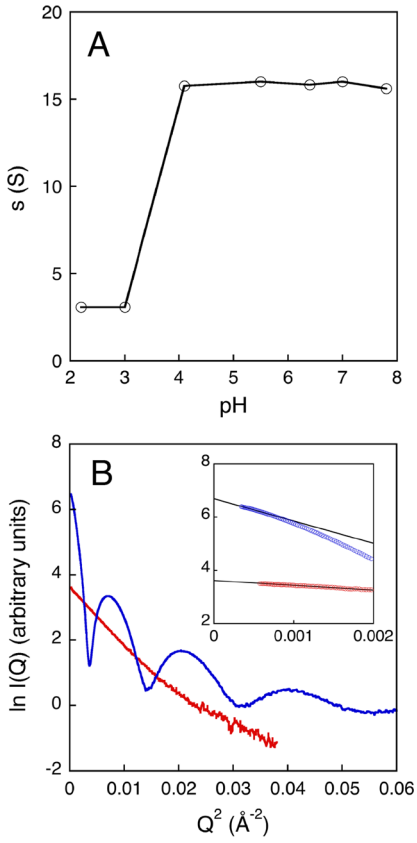

Figure 2. pH dependence of the sedimentation coefficient and SAXS. (A) Sedimentation coefficient (s) of EcFtnA as a function of pH. (B) Guinier plots of EcFtnA at pH 7 (blue) and pH 2.5 (red). The scattering profiles obtained at protein concentrations of 4 and 2 mg/mL are shown as examples for pH 7 and 2.5, respectively. The inset is an expansion of the low-Q^2 region, where the radii of gyration were calculated by the Guinier approximation (—).

Table 1. Sedimentation Coefficients of EcFtnA and Its Mutants

	pH 7	pH 3
WT	15.24	2.94
H106A	14.95	2.99
H106P	2.89	2.87[a]
F117A	15.11 and 2.96	3.00
H128A	14.91	15.00 and 2.93
146Δ	16.40	2.91[a]
139Δ	2.83[a]	2.84[a]

[a]The measurement was performed under nonsalt conditions.

DOI: 10.1021/acs.biochem.5b00723
Biochemistry 2015, 54, 6243−6251

Å from the coordinates of subunits A and F. This value shows fair agreement with the value observed at pH 2.5. Because other possible pairs of subunits found in the 24-mer (AC, AD, AO, and AX) gave radii of gyration of 26−28 Å (see Figure S1), we concluded that the dyad-related dimer is stable under acidic conditions.

We also investigated the pH dependence of the secondary and tertiary structures of EcFtnA by measuring the far- and near-UV CD spectra (Figure 3). The far-UV CD spectra of

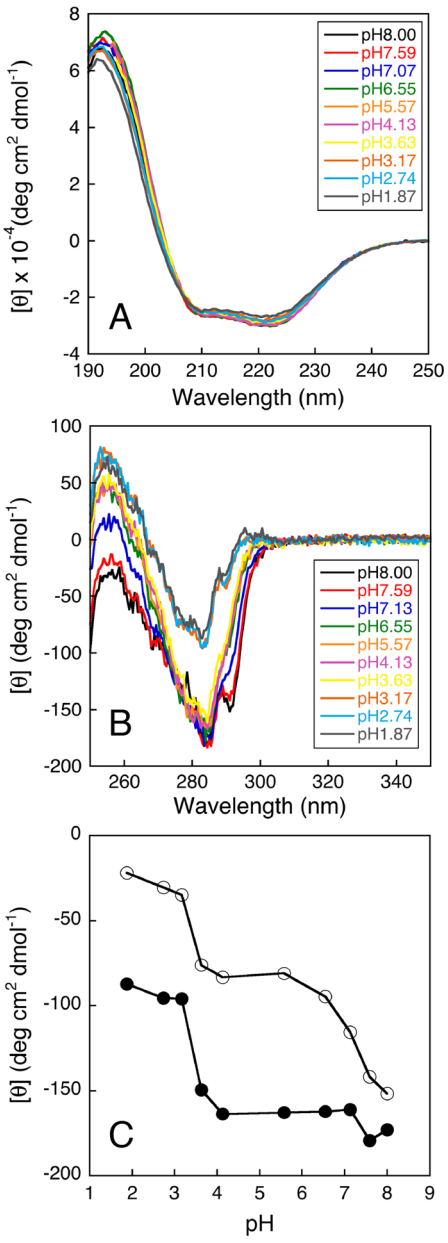

Figure 3. pH dependence of (A) far-UV and (B) near-UV CD spectra for EcFtnA. (C) CD intensities at 291 and 283 nm are represented by empty and filled circles, respectively.

EcFtnA showed typical helical features and were substantially unchanged in the pH range of 2−8 (Figure 3A), indicating that the secondary structure in the dimer was similar to that in the 24-mer of EcFtnA. By contrast, the near-UV CD spectra were dependent on pH (Figure 3B,C). Two negative peaks were observed at 291 and 283 nm in the spectrum at pH 8. The peak at 291 nm disappeared at pH 6. Because the sedimentation coefficients suggested that the 24-mer was maintained in the pH range of 4−8, the spectral change between pH 8 and 6 may reflect the protonation of side chains close to the aromatic residues, which cause the negative peak at 291 nm (probably tryptophan residues). There are two tryptophan residues (30 and 122) in EcFtnA. The most plausible residue that is protonated between pH 8 and 6 is histidine. H34 is close to W30 (the distance between H34 Nε2 and W30 Cε2 is 3.22 Å), and H53 is close to W122 (the distance between H53 Cγ and W122 Cη2 is 4.17 Å). The protonation of H34 and/or H53 is likely to be the reason for the CD spectrum change between pH 8 and 6. The peak intensities at 291 and 283 nm in the near-UV CD spectra were reduced between pH 4 and 3. Because the sedimentation coefficient also decreased in this pH range (Figure 2), this spectral change likely reflects the dissociation of the 24-mer. Even at pH 2, a negative peak at 283 nm and a positive peak at 254 nm remained, which suggests that tryptophan side chains are buried inside the rigid tertiary structure of the dimer subunit.

The results of the analytical ultracentrifugation (AUC), SAXS, and CD measurements revealed that the 24-meric EcFtnA dissociated into the dimer below pH 3 (Figure 2A) and that the dimeric EcFtnA retained the nativelike secondary and tertiary structures at acidic pH (Figure 3). This behavior is similar to the properties of mammalian ferritins studied so far.[17−19] Bfrs exist in an equilibrium mixture of a 24-mer and a dimer, even under physiological conditions.[10,11] Therefore, we can conclude that the dimer is a basic unit of all 24-meric nanocages.

CD Spectra of EcFtnA Mutants. We constructed two series of mutants to investigate the important intersubunit interactions when 12 dimers associate to form a 24-meric nanocage. One series of mutants consisted of H106A, H106P, F117A, and H128A, which have mutations at residues near the 3-fold axis. The mutation in H106 is located on helix C, and those of F117 and H128 are located on helix D (Figure 1A). These residues were selected after considering the results of virtual alanine scanning.[28] The other series of mutants consisted of 139Δ (residues 1−138) and 146Δ (residues 1−145), which are truncated mutants that lack the residues near the 4-fold axis. 146Δ completely lacks helix E, and 139Δ lacks the C-terminal sequence of helix D (Figure 1B).

At pH 7, the far-UV CD spectra of these mutants were similar to those of WT, although the spectrum intensities of H106P (Figure 4A) and 146Δ (Figure 4B) were slightly reduced. The H106P mutation may disrupt helix C in which H106 is located. Note that the spectra are presented as the mean residue ellipticity. Although helical residues should be removed in the truncated mutant, nonhelical residues may also be removed, so that the average helicity may not change significantly. The observation that the CD intensity of 146Δ was reduced but that of 139Δ was not may reflect the fact that the helical residues were predominantly removed in 146Δ. Although the near-UV CD spectra of H106A, H128A, and 146Δ were similar to the spectrum of WT, the spectra of H106P, F117A (Figure 4C), and 139Δ (Figure 4D) were different from the spectrum of WT. Thus, the tertiary or quaternary structure of H106P, F117A, and 139Δ seems to be largely deformed.

At pH 3, the near- and far-UV CD spectra of the mutants except for H106P and 139Δ were similar to those of WT (Figure 4E−H). Because all mutants existed as dimers at pH 3

DOI: 10.1021/acs.biochem.5b00723
Biochemistry 2015, 54, 6243−6251

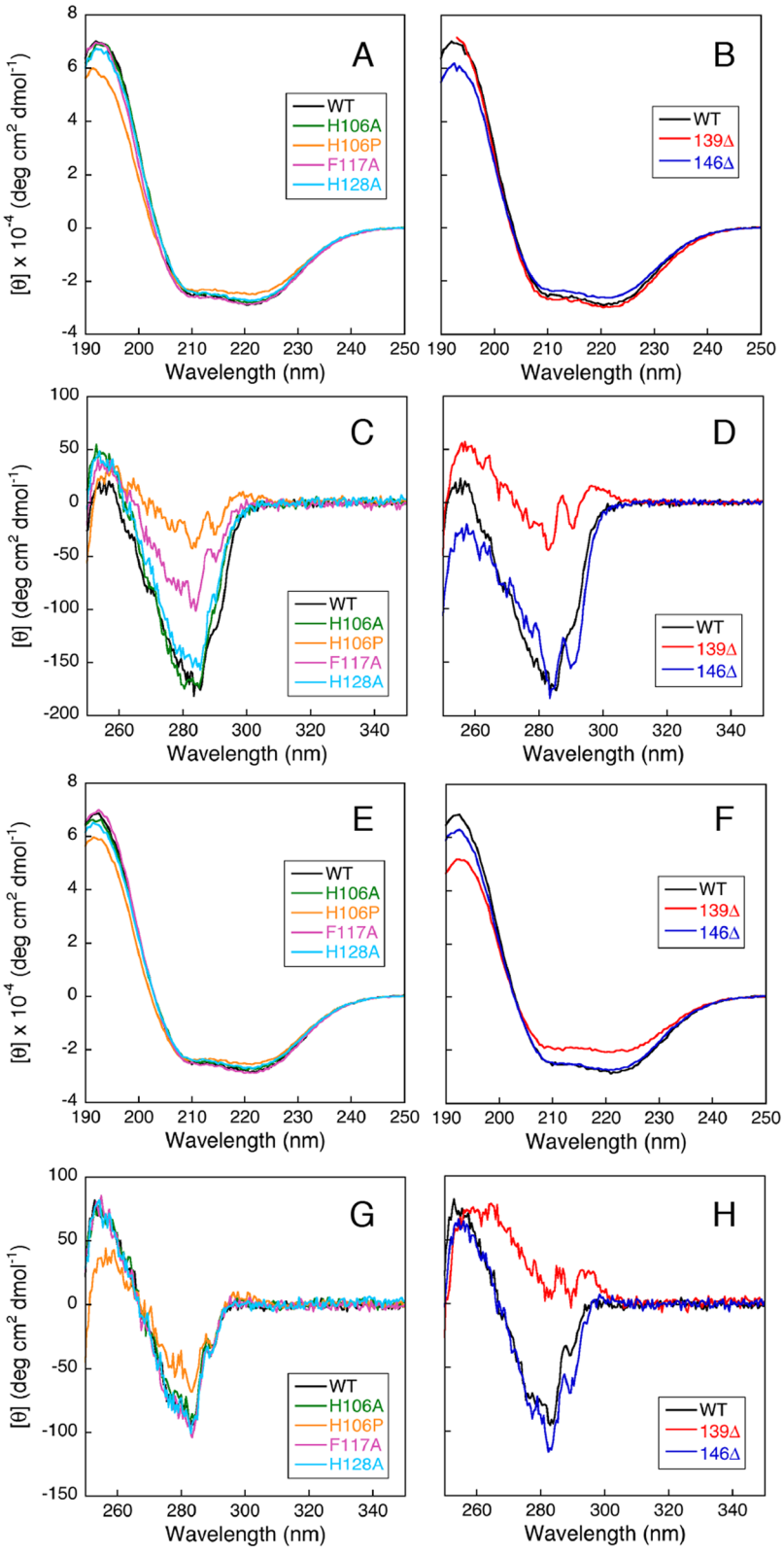

Figure 4. Far- and near-UV CD spectra of WT and mutants measured at (A–D) pH 7 and at (E–H) pH 3. For the sake of clarity, panels A, C, E, and G compare the spectra of the 3-fold axis mutants, H106A (green), H106P (orange), F117A (pink), and H128A (sky blue), with that of WT (black). In panels B, D, F, and H, the spectra of the 4-fold axis mutants, 139Δ (red) and 146Δ (blue), are compared with that of WT (black).

(see below), most point mutations and truncation of the C-terminal 20 residues (146Δ) did not affect the dimer structure. The substitution of H106 with a proline residue must disrupt helix C, at least partly, because the proline cannot establish a hydrogen bond with the fourth residue located before this position. Because the far- and near-UV CD spectra differed significantly between 139Δ and WT, we conclude that the C-terminal truncation of seven additional residues (the C-

DOI: 10.1021/acs.biochem.5b00723
Biochemistry 2015, 54, 6243–6251

terminus of helix D) disrupted the secondary and tertiary structures of the dimer. This is interesting because helix D is far from the dimer interface (see Discussion).

Oligomeric States of WT and Mutants. Gel filtration chromatography was performed to identify the oligomeric states of the EcFtnA mutants (Figure 5). 139Δ was not analyzed because it precipitated under the chromatograph conditions [20 mM PIPES (pH 7) containing 200 mM NaCl]. Mutants H106A and H128A eluted as a single peak at an elution time identical to that of WT, indicating that H106A and H128A are 24-meric. Although the elution of 146Δ was indistinguishable from that of 24-meric ferritin, the results of AUC suggested that 146Δ formed oligomers larger than 24-meric ferritin (see below). By contrast, F117A existed as an equilibrium mixture of the dimer and 24-mer, indicating that F117 contributed significantly to 24-mer formation. H106P completely dissociated to a dimer. It is likely that H106P mutation disrupts the C-terminus of helix C, as indicated by the reduced CD intensity (Figure 4A), which induces a large conformational change in the interface near the 3-fold axis.

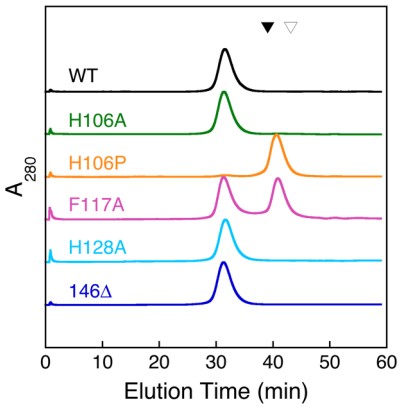

Figure 5. Gel filtration analysis of WT and mutants. Elution profiles from a Superose 6 column (1 cm × 30 cm) of WT, H106A, H106P, F117A, H128A, and 146Δ. The elution times of ovalbumin (43 kDa) and chymotrypsinogen A (25 kDa) are represented by the filled triangle and empty triangle, respectively.

AUC was also performed at pH 7 [10 mM sodium phosphate (pH 7) containing 200 mM NaCl] and pH 3 [10 mM sodium phosphate (pH 3) containing 200 mM NaCl] (Table 1). Because 139Δ (pH 3 and 7), 146Δ (pH 3), and H106P (pH 3) precipitated at high salt concentrations, their measurements were performed under nonsalt conditions (50 mM sodium phosphate). At pH 7, H106A and H128A showed a single sedimentation coefficient identical to that of WT (Table 1). By contrast, H106P and 139Δ showed a single sedimentation coefficient identical to that of the WT dimer manifested at pH 3 (Table 1). F117A showed two sedimentation coefficients that corresponded to the 24-mer and dimer (Table 1 and Figure S2). These results were consistent with those of the gel filtration experiment. The sedimentation coefficient of 146Δ (16.4 S) was slightly larger than that of the 24-mer (Table 1). Inspection of the $c(s)$ distribution of 146Δ (Figure S2) revealed that there were at least two components of 14 and 17 S. Therefore, it seems that 146Δ existed as a mixture of 24-mer and larger oligomers.

At pH 3, all mutants existed as a dimer as did WT. Unexpectedly, the significant population of the 24-mer was observed on the $c(s)$ distribution of H128A at pH 3 (Figure S2). Although it was expected that the H128A mutation would reduce the net charge at pH 3 and suppress the repulsion between subunits, this should also have occurred in H106A. Therefore, we conclude that this did not occur because of reduced electrostatic repulsion between the net charges of the subunits but was instead a result of local electrostatic repulsions or a result of favorable interactions between A128 and nearby residues.

Thermal Denaturation of WT and Mutants. The thermal denaturation was monitored by CD at 222 nm (Figure 6). WT was extremely stable and did not completely denature at 90 °C. The results of gel filtration and AUC suggest that the melting curves of H106A, H128A, and 146Δ are likely to reflect the stability of the 24-mer, whereas those of H106P and 139Δ reflect the stability of the dimer. The melting curve of F117A may also reflect the stability of the dimer, because F117A is expected to exist as a dimer at higher temperatures, although it exists as an equilibrium mixture of the 24-mer and dimer at ambient temperatures. The CD values of H106A and H128A increased at a temperature lower than that of WT, suggesting that both H106 and H128 involved 24-mer stabilizing interactions. The contribution of helix E at the 4-fold axis seems to be not so large because the stability of the 20-residue truncated mutant (146Δ) was similar to that of a point mutant (H106A). The melting temperature was lower for H106P than for 139Δ, although neither residue 106 nor residues 139−165 seemed to be involved in the dyad-related dimer interface. This difference probably originates from the difference in the extent to which the mutations affect the monomer conformation.

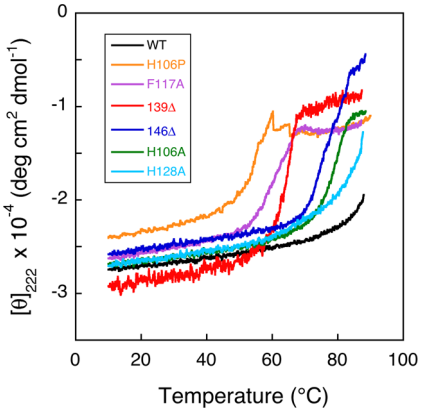

Figure 6. Thermal denaturation curves for WT and mutants monitored by far-UV CD at 222 nm.

Iron Storage of WT and Mutants. An iron storage experiment was performed to investigate the influence of mutations and C-terminal truncations. Native PAGE was performed for EcFtnA before (Figure 7A) and after (Figure 7B,C) incubation with ∼250 iron ions per nanocage, and the gels were stained with Coomassie brilliant blue (Figure 7A,B) and Prussian blue (Figure 7C). In the absence of iron, H106P showed a single band with a mobility that was larger than that of the WT (Figure 7A), which probably corresponds to the dimer. This result is consistent with the results of the gel filtration and AUC experiments and indicates that H106P is not able to form a nanocage. F117A showed two bands corresponding to the 24-mer and the dimer (Figure 7A). This result is also consistent with the results of the gel filtration and AUC experiments and suggests that F117A is in

DOI: 10.1021/acs.biochem.5b00723
Biochemistry 2015, 54, 6243−6251

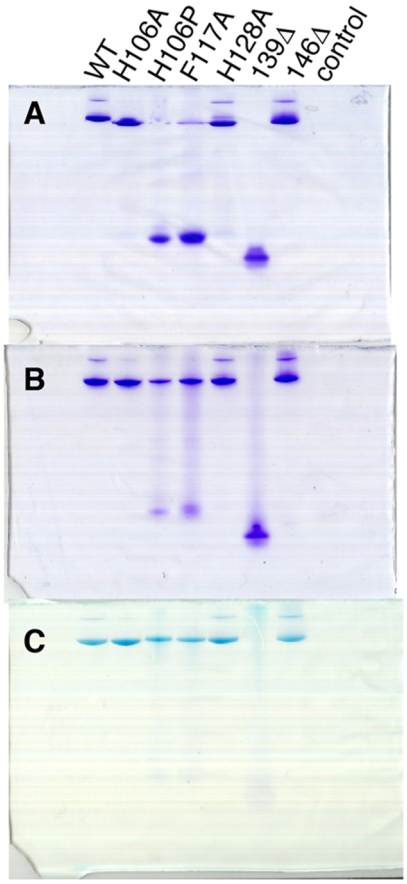

Figure 7. Analysis of iron storage for WT and mutants. Native PAGE was performed (A) before and (B and C) after incubation with ~250 iron ions per nanocage. The gels were stained with (A and B) Coomassie brilliant blue and (C) Prussian blue. Control represents the iron storage analysis in the absence of protein.

equilibrium between the 24-mer and the dimer. It is of interest that the bands corresponding to the 24-mer became clear, and that the band corresponding to the dimer became a smear after incubation with iron (Figure 7B). This indicates that the 24-mer was induced by incubation with iron. Because Prussian blue staining was observed for all bands with the mobility of the 24-mer (Figure 7C), we can conclude that all mutants except 139Δ have iron-incorporating ability and that the nanocages of H106P and F117A are stabilized by the formed iron core.

DISCUSSION

Contribution of the Interface near the 4-Fold Axis to 24-mer Stability. To address the contribution of the interface around the 4-fold axis, two truncated mutants 146Δ and 139Δ were constructed in this study. 146Δ was able to form a 24-meric structure and to incorporate iron. Therefore, the 20 C-terminal residues, which form helix E, were not essential for forming the 24-mer nanocage. However, these residues seemed to endow EcFtnA with fidelity of the 24-mer formation because the AUC experiments showed that 146Δ could form larger aggregates in addition to the 24-mer (Figure S2). Similar results have been reported for mammalian ferritins. Residue 146 of EcFtnA corresponds to residue 162 of HuHF.[16] Levi et al.[29] have shown that a mutant of HuHF, rH-P161-am, in which the residues beyond 160 were deleted, assembled into a nativelike nanocage. Similar results were also reported for the truncated mutant of mouse ferritin chain H.[30] The remarkable difference is that the iron-incorporating ability of these mammalian mutants was lost by truncation of helix E. The difference in iron-incorporating ability between the truncated mutants of mammalian and *E. coli* ferritins may reflect the fact that both chains H and L are responsible for the iron-incorporating function in mammalian ferritins. It has been reported that Bfrs from *E. coli* and *M. tuberculosis* exist as an equilibrium mixture between the dimer and the 24-mer.[10,11] This means that the 24-mers of Bfrs are less stable than those of non-heme-binding ferritins. Although an *E. coli* Bfr mutant lacking helix E is unable to form a 24-mer,[31] in contrast to helix E-truncated non-heme-binding ferritins, this was not a surprising result considering the intrinsic instability of the Bfr nanocage.

AUC and native PAGE showed that 139Δ was unable to form the 24-mer nanocage (Table 1 and Figure 7). Because the sedimentation coefficient is the same at pH 7 and 3, it is reasonable to conclude that 139Δ exists as a dimer. The far-UV CD spectra showed that the secondary structure was similar in 139Δ and WT. Thermal denaturation experiments showed that 139Δ was denatured cooperatively (Figure 6), suggesting that 139Δ has a rigid tertiary structure. These results suggest that 139Δ maintains a nativelike dimer structure but loses the ability to form the 24-mer and that the seven residues from position 139 to 145 are important for 24-mer formation. A truncated HuHF, which lacked residues beyond L155 (corresponding to L141 of EcFtnA), was unable to form 24-mer.[13,32] Therefore, the C-terminus of helix D seems to be important for 24-mer formation. By contrast, the C-terminus of helix D is not essential for dimer formation. At pH 3, the near- and far-UV CD spectra of 139Δ differed significantly from those of WT (panels H and F of Figure 4, respectively), but the sedimentation coefficient showed that 139Δ was a dimer (Table 1). This suggests that 139Δ maintained a nativelike dimer interface comprising helix A, helix B, and loop BC, although the helical content was significantly reduced. Because the CD spectrum of 139Δ was similar to that of WT at pH 7 (Figure 4B), the helix destabilized at pH 3 may be stabilized at pH 7 by some electrostatic interactions.

Contribution of the Interface near the 3-Fold Axis to 24-mer Stability. Of the residues near the 3-fold axis, H106, Y114, F117, N118, Q121, V124, and H128 were predicted to be "hot spot" residues by virtual alanine scanning.[28] In this study, H106A, F117A, and H128A substitutions were examined experimentally. Both H106A and H128A were 24-meric, and their secondary and tertiary structures were similar to that of WT as judged by the CD spectra. Because the thermal stability was reduced for both mutants, H106 and H128 made some contributions to the stabilization of the 24-mer. Although crystallographic analysis has shown that H106 Nδ1 and H128 Nε2 make a hydrogen bond with Y114 OH and Asp63 Oδ1 of neighboring chains, respectively,[16] they seem not to be essential. The F117A mutation has a somewhat larger effect because F117A was in equilibrium between the dimer and 24-mer, possibly because F117 interacted with the F117 residues of two other subunits just at the 3-fold axis. F117 also interacted with Y114 of neighboring chains, which is also predicted to be a hot spot. Therefore, F117A substitution had multiple effects on hot spot residues. Although the near-UV CD intensity was significantly reduced in F117A at pH 7 (Figure 4C), this is probably not related to the tertiary structure change but to the dissociation-induced change in the CD

DOI: 10.1021/acs.biochem.5b00723
Biochemistry 2015, 54, 6243−6251

contribution of Y114 because the near-CD spectrum of F117A was the same as that of WT at pH 3 (Figure 4G).

H106P was designed to introduce a large perturbation into the interface around the 3-fold axis. Because H106 is located at the C-terminus of helix C, its substitution with proline was expected to disrupt helix C, at least partially. As expected, the helical content of H106P was reduced (Figure 4A), and H106P was unable to form the 24-mer (Table 1 and Figure 5). The displacement of residues that interact with neighboring subunits was probably induced by the unfolding of helix C. As in the case of 139Δ, which disrupts helix D, the perturbation of helix C seems not to disturb dimer formation.

CONCLUSION

This study was the first mutational analysis of the intersubunit interactions of a bacterial non-heme-binding ferritin. A comparison with results obtained for mammalian ferritins revealed the following common principles of 24-meric nanocage formation. First, the 2-fold symmetry-related dimer is the most stable building block of the 24-mer. Second, interactions near the 3-fold symmetry axis seem to be cumulative, although the contribution of each interaction is not large. Finally, helix E at the 4-fold symmetry axis is not essential for nanocage formation. A striking difference between bacterial and mammalian ferritins was that helix E-truncated EcFtnA maintained an iron-incorporating ability, whereas mammalian mutants lost it.

ASSOCIATED CONTENT

Supporting Information

The Supporting Information is available free of charge on the ACS Publications website at DOI: 10.1021/acs.biochem.5b00723.

Supplementary Figures S1 and S2 (PDF)

AUTHOR INFORMATION

Corresponding Author

*E-mail: ikeguchi@soka.ac.jp. Phone: +81-426-91-9444.

Present Addresses

[§]H.O.: Graduate School of Medical Life Science, Yokohama City University, 1-7-29 Suehiro-cho, Tsurumi-ku, Yokohama 230-0045, Japan.

[∥]Y.M.: School of Life Sciences, Tokyo University of Pharmacy and Life Sciences, 1432-1 Horinouchi, Hachioji, Tokyo 192-0392, Japan.

Funding

This work was supported in part by the Science Research Promotion Fund (M.I., 2010) from the Promotion and Mutual Aid Corporation for Private Schools of Japan.

Notes

The authors declare no competing financial interest.

ACKNOWLEDGMENTS

We thank Dr. Yuko H. Itoh for providing genomic DNA of the *E. coli* B strain. The synchrotron radiation SAXS experiments were performed at BL-15A and BL-6A of the Photon Factory with the approval of the High Energy Accelerator Research Organization (Proposals 2009G620 and 2011G689) and at BL45XU of SPring-8 with the approval of the Japan Synchrotron Radiation Research Institute (JASRI) (Proposals 2011A1133, 2012A1217, and 2012B1114). We thank Dr. Takaaki Hikima of RIKEN for assistance with the beamline alignment.

ABBREVIATIONS

EcFtnA, *E. coli* non-heme-binding ferritin A; HuHF, human ferritin H; Bfr, bacterioferritin; Dps, DNA-binding protein from starved cells; AUC, analytical ultracentrifugation; SAXS, small-angle X-ray scattering; PDB, Protein Data Bank.

REFERENCES

(1) Arosio, P., and Levi, S. (2010) Cytosolic and mitochondrial ferritins in the regulation of cellular iron homeostasis and oxidative damage. *Biochim. Biophys. Acta, Gen. Subj. 1800*, 783−792.

(2) Le Brun, N. E., Crow, A., Murphy, M. E., Mauk, A. G., and Moore, G. R. (2010) Iron core mineralisation in prokaryotic ferritins. *Biochim. Biophys. Acta, Gen. Subj. 1800*, 732−744.

(3) Chiancone, E., and Ceci, P. (2010) The multifaceted capacity of Dps proteins to combat bacterial stress conditions: Detoxification of iron and hydrogen peroxide and DNA binding. *Biochim. Biophys. Acta, Gen. Subj. 1800*, 798−805.

(4) Crichton, R. R., and Declercq, J. P. (2010) X-ray structures of ferritins and related proteins. *Biochim. Biophys. Acta, Gen. Subj. 1800*, 706−718.

(5) Zhang, Y., and Orner, B. P. (2011) Self-assembly in the ferritin nano-cage protein superfamily. *Int. J. Mol. Sci. 12*, 5406−5421.

(6) Uchida, M., Kang, S., Reichhardt, C., Harlen, K., and Douglas, T. (2010) The ferritin superfamily: Supramolecular templates for materials synthesis. *Biochim. Biophys. Acta, Gen. Subj. 1800*, 834−845.

(7) Yamashita, I., Iwahori, K., and Kumagai, S. (2010) Ferritin in the field of nanodevices. *Biochim. Biophys. Acta, Gen. Subj. 1800*, 846−857.

(8) Huard, D. J., Kane, K. M., and Tezcan, F. A. (2013) Re-engineering protein interfaces yields copper-inducible ferritin cage assembly. *Nat. Chem. Biol. 9*, 169−176.

(9) Otsuka, S., Listowsky, I., Niitsu, Y., and Urushizaki, I. (1980) Assembly of intra- and interspecies hybrid apoferritins. *J. Biol. Chem. 255*, 6234−6237.

(10) Khare, G., Nangpal, P., and Tyagi, A. K. (2013) Unique residues at the 3-fold and 4-fold axis of mycobacterial ferritin are involved in oligomer switching. *Biochemistry 52*, 1694−1704.

(11) Zhang, Y., Raudah, S., Teo, H., Teo, G. W., Fan, R., Sun, X., and Orner, B. P. (2010) Alanine-shaving mutagenesis to determine key interfacial residues governing the assembly of a nano-cage maxi-ferritin. *J. Biol. Chem. 285*, 12078−12086.

(12) Zhang, Y., Fu, J., Chee, S. Y., Ang, E. X., and Orner, B. P. (2011) Rational disruption of the oligomerization of the mini-ferritin E. coli DPS through protein-protein interface mutation. *Protein Sci. 20*, 1907−1917.

(13) Levi, S., Luzzago, A., Franceschinelli, F., Santambrogio, P., Cesareni, G., and Arosio, P. (1989) Mutational analysis of the channel and loop sequences of human ferritin H-chain. *Biochem. J. 264*, 381−388.

(14) Jappelli, R., Luzzago, A., Tataseo, P., Pernice, I., and Cesareni, G. (1992) Loop mutations can cause a substantial conformational change in the carboxy terminus of the ferritin protein. *J. Mol. Biol. 227*, 532−543.

(15) Santambrogio, P., Pinto, P., Levi, S., Cozzi, A., Rovida, E., Albertini, A., Artymiuk, P., Harrison, P. M., and Arosio, P. (1997) Effects of modifications near the 2-, 3- and 4-fold symmetry axes on human ferritin renaturation. *Biochem. J. 322* (2), 461−468.

(16) Stillman, T. J., Hempstead, P. D., Artymiuk, P. J., Andrews, S. C., Hudson, A. J., Treffry, A., Guest, J. R., and Harrison, P. M. (2001) The high-resolution X-ray crystallographic structure of the ferritin (EcFtnA) of Escherichia coli; comparison with human H ferritin (HuHF) and the structures of the Fe(3+) and Zn(2+) derivatives. *J. Mol. Biol. 307*, 587−603.

(17) Crichton, R. R., and Bryce, C. F. (1973) Subunit interactions in horse spleen apoferritin. Dissociation by extremes of pH. *Biochem. J. 133*, 289−299.

DOI: 10.1021/acs.biochem.5b00723
Biochemistry 2015, 54, 6243−6251

(18) Linder, M. C., Kakavandi, H. R., Miller, P., Wirth, P. L., and Nagel, G. M. (1989) Dissociation of ferritins. *Arch. Biochem. Biophys. 269*, 485−496.
(19) Stefanini, S., Cavallo, S., Wang, C. Q., Tataseo, P., Vecchini, P., Giartosio, A., and Chiancone, E. (1996) Thermal stability of horse spleen apoferritin and human recombinant H apoferritin. *Arch. Biochem. Biophys. 325*, 58−64.
(20) Gill, S. C., and von Hippel, P. H. (1989) Calculation of protein extinction coefficients from amino acid sequence data. *Anal. Biochem. 182*, 319−326.
(21) Schuck, P. (2000) Size-distribution analysis of macromolecules by sedimentation velocity ultracentrifugation and lamm equation modeling. *Biophys. J. 78*, 1606−1619.
(22) Nakagawa, K., Yamada, Y., Matsumura, Y., Tsukamoto, S., Yamamoto-Ohtomo, M., Ohtomo, H., Okabe, T., Fujiwara, K., and Ikeguchi, M. (2014) Relationship between chain collapse and secondary structure formation in a partially folded protein. *Biopolymers 101*, 651−658.
(23) Arai, M., Ito, K., Inobe, T., Nakao, M., Maki, K., Kamagata, K., Kihara, H., Amemiya, Y., and Kuwajima, K. (2002) Fast compaction of alpha-lactalbumin during folding studied by stopped-flow X-ray scattering. *J. Mol. Biol. 321*, 121−132.
(24) Hammersley, A. P., Svensson, S. O., Hanfland, M., Fitch, A. N., and Hausermann, D. (1996) Two-dimensional detector software: From real detector to idealised image or two-theta scan. *High Pressure Res. 14*, 235−248.
(25) Banyard, S. H., Stammers, D. K., and Harrison, P. M. (1978) Electron density map of apoferritin at 2.8-A resolution. *Nature 271*, 282−284.
(26) Fujiwara, K., and Ikeguchi, M. (2008) OLIGAMI: OLIGomer Architecture and Molecular Interface. *Open Bioinf. J. 2*, 50−53.
(27) Svergun, D., Barberato, C., and Koch, M. H. J. (1995) CRYSOL - A program to evaluate x-ray solution scattering of biological macromolecules from atomic coordinates. *J. Appl. Crystallogr. 28*, 768−773.
(28) Kortemme, T., Kim, D. E., and Baker, D. (2004) Computational alanine scanning of protein-protein interfaces. *Sci. Signaling 2004*, pl2.
(29) Levi, S., Luzzago, A., Cesareni, G., Cozzi, A., Franceschinelli, F., Albertini, A., and Arosio, P. (1988) Mechanism of ferritin iron uptake: activity of the H-chain and deletion mapping of the ferro-oxidase site. A study of iron uptake and ferro-oxidase activity of human liver, recombinant H-chain ferritins, and of two H-chain deletion mutants. *J. Biol. Chem. 263*, 18086−18092.
(30) Ingrassia, R., Gerardi, G., Biasiotto, G., and Arosio, P. (2006) Mutations of ferritin H chain C-terminus produced by nucleotide insertions have altered stability and functional properties. *J. Biochem. 139*, 881−885.
(31) Fan, R., Boyle, A. L., Cheong, V. V., Ng, S. L., and Orner, B. P. (2009) A helix swapping study of two protein cages. *Biochemistry 48*, 5623−5630.
(32) Luzzago, A., and Cesareni, G. (1989) Isolation of point mutations that affect the folding of the H chain of human ferritin in E.coli. *EMBO J. 8*, 569−576.

DOI: 10.1021/acs.biochem.5b00723
Biochemistry 2015, 54, 6243−6251